Relativistic electron dynamics in a cusped magnetic field

M. J. Rhee and W. W. Destler

University of Maryland, College Park, Maryland 20742

(Received 30 January 1974)

Single-particle motion of relativistic electrons in a cusped magnetic field has been studied both analytically and experimentally. The Lagrangian formulation is used to solve for the electron trajectories in some simple magnetic cusp configurations. A threshold energy for transmission through the cusp is found, and confirmed experimentally. Two different electron orbit off-centering mechanisms are discussed; one arising from a nonzero radial component of particle velocity on the upstream side of the cusp transition, and another arising from the finite width of the cusp transition. Experiments are reported confirming the existence of these off-centering mechanisms, and the results are compared with theoretical expectations.

I. INTRODUCTION

Renewed interest in charged-particle dynamics in cusped magnetic field configurations has resulted from recent applications of cusp fields to problems of plasma heating and collective ion acceleration. In particular, the nonadiabatic trajectories of charged particles in cusp fields allow an efficient conversion of longitudinal particle velocity to rotational velocity, and make possible the use of such field configurations for the generation of strong E layers and electron rings with properties attractive for ion heating and acceleration.

Early work on the nonadiabatic motion of nonrelativistic charged particles in cusped magnetic fields was reported by Schmidt,[1] who analyzed the possible trajectories of particles injected into a magnetic cusp. This work predicted the existence of a threshold velocity for transmission through the cusp, as well as a qualitative description of possible particle orbits after the cusp transition. Experimental work confirming much of this early analysis was performed by Sinnis *et al.*,[2] who reported experiments on nonrelativistic particle dynamics using a low current beam of 2 keV electrons.

The use of magnetic cusps for the generation of strong, rotating electron rings and E layers was investigated by Nelson, Kalnins, and Kim,[3,4] who reported computational and analytical studies of particle trajectories assuming simplified cusp geometries. Possible magnetic field configurations and a preliminary analysis of the use of such rotating rings for collective ion acceleration were reported by Reiser.[5,6]

The first experimental work in which an intense, relativistic electron beam was injected through a magnetic cusp was reported by Friedman.[7] His work suggested that the injection of very short duration, high current beams of relativistic electrons into cusped field configurations might provide an attractive alternate method of forming intense rotating electron rings and E layers. Recently, several experiments have been reported in which intense, relativistic electron beams were injected through magnetic cusps. Kapetenakos *et al.*,[8] have reported a plasma heating experiment in which a significant fraction of the beam energy is transferred to a background plasma after transmission through a magnetic cusp. In addition, Kribel *et al.*[9] have succeeded in producing field reversing E layers using cusp injection. Preliminary results of the work presented here have been previously reported.[10–12]

In Sec. II of this paper the Lagrangian formulation is used to solve for the relativistic particle trajectories in some simplified cusp configurations. Section III presents the experimental work performed to check the theory, and results are compared. Final conclusions are drawn in Sec. IV.

II. THEORETICAL DISCUSSION

The Lagrangian for the motion of relativistic electrons in the presence of external axisymmetric electric and magnetic fields may be written as

$$L = -m_0c^2\left(1 - \frac{\dot{r}^2 + r^2\dot{\theta}^2 + \dot{z}^2}{c^2}\right)^{1/2} + e\phi - er\dot{\theta}A_\theta, \qquad (1)$$

where m_0 is the electron rest mass, c is the velocity of light in vacuum, e is the electronic charge, and ϕ is the scalar potential (rationalized mks units are used throughout). A_θ is the only nonzero component of the magnetic vector potential if the magnetic field is produced by axisymmetric coils.

The Lagrange equations follow immediately from the above relation and may be used to solve for the motion of the electron in various field configurations. In many cases, however, the nonlinearity and coupled nature of Lagrange equations increase the difficulty in finding analytic solutions. In this section solutions of these equations will be found for two different cusp-field configurations.

A. Ideal cusp

Figure 1 shows schematically a fully-idealized cusp field configuration. A hollow electron beam is emitted from a circular cathode centered on the axis of symmetry of the cusp, and the beam is accelerated in the anode–cathode gap before the cusp transition. An infinitely small cusp transition is assumed and the magnetic field as a function of axial position z may be written

$$B_z = B_{z0}[1 - 2u(z)] \qquad (2a)$$

and accordingly

$$A_\theta = \frac{rB_{z0}}{2}[1 - 2u(z)] \qquad (2b)$$

where u is the Heaviside unit step function. The actual experimental cusp transition width is sufficiently small (about

Copyright © 1974 American Institute of Physics

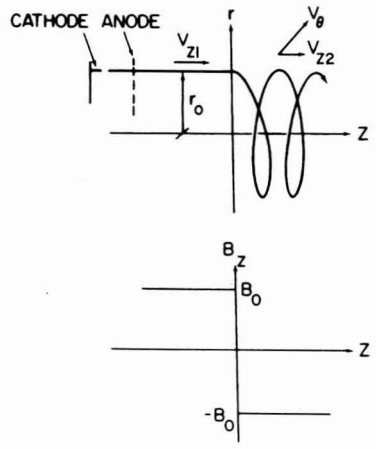

FIG. 1. Fully idealized cusp field configuration.

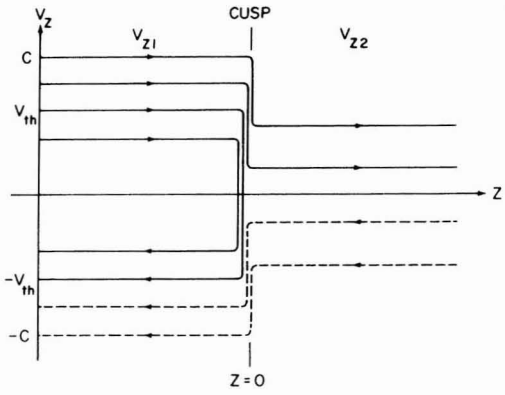

FIG. 2. Ideal cusp phase space trajectories.

1.5 cm) so that the assumption of such an idealized field configuration is not an unreasonable starting point for the theoretical development.

In this case, the Lagrange equation for the θ coordinate becomes

$$P_\theta \equiv m_0\gamma r^2\dot{\theta} - erA_\theta = \text{const}, \tag{3}$$

where

$$\gamma = \left(1 - \frac{v^2}{c^2}\right)^{-1/2}.$$

Relation (3) is simply an expression for the conservation of canonical angular momentum in an axisymmetric system. An axisymmetric electric field in the diode will affect only the value of γ.

The constant in Eq. (3) may be evaluated from the following initial conditions at the cathode:

(i) $r = r_0$,

(ii) $A_\theta = r_0 B_{z0}/2$ [from Eq. (2)],

(iii) $\dot{\theta} = 0$ [assuring that there is no θ component of electric field in the diode region].

Thus at $t = 0$,

$$P_\theta = -\frac{er_0^2 B_{z0}}{2}$$

and Eq. (3) can be rewritten

$$r^2\dot{\theta} = \frac{\omega_c}{2}[r^2(1 - 2u) - r_0^2], \tag{4}$$

where $\omega_c = eB_{z0}/\gamma m_0$ is the relativistic electron cyclotron frequency. Assuming that γ is constant after the initial electron acceleration in the diode, this result may be used to decouple the Lagrange equation for the z coordinate from the azimuthal motion, with the result

$$\ddot{z} - \frac{\omega_c^2}{2}[r^2(1 - 2u) - r_0^2]\delta(z) = 0, \tag{5}$$

where $\delta(z)$ is the Dirac delta function arising from the very narrow radial component of magnetic field at the cusp transition.

Equation (5) may be easily integrated using

$$\frac{d}{dt} = v_z\frac{d}{dz}$$

to separate the variables v_z and z. If the initial axial velocity on the upstream side of the cusp is v_{z1} and the axial velocity downstream is v_{z2}, Eq. (5) yields

$$v_{z2}^2 = v_{z1}^2 - r_0^2\omega_c^2. \tag{6}$$

Thus, the change in axial velocity across the cusp transition is independent of the radial position of the electron as it passes through the cusp.

The trajectories of Eq. (6) in phase space are shown in Fig. 2. There exists a threshold velocity, given by

$$v_{zth} = r_0\omega_c$$

below which electrons will be reflected at the cusp. This result is identical to that found by Schmidt[1] for the nonrelativistic case. Electrons with velocities above this threshold value pass through the cusp with downstream axial velocity given by Eq. (6).

The Lagrange equation for the radial component may be written

$$\ddot{r} + r\frac{\omega_c^2}{4}\left((1 - 2u)^2 - \frac{r_0^4}{r^4}\right) = 0. \tag{7a}$$

At every point excluding $z = 0$ (the cusp transition point), the term $(1 - 2u)^2$ reduces to unity. Equation (7a) may then be written in the simpler form

$$\ddot{r} + r\frac{\omega_c^2}{4}\left(1 - \frac{r_0^4}{r^4}\right) = 0. \tag{7b}$$

The nonlinearity of this differential equation makes an analytic solution quite difficult. Equation (7b), however, has the same form as the equation of motion of a point in space with circular motion of constant angular frequency ω, radius of gyration ρ, and center of gyration a distance R

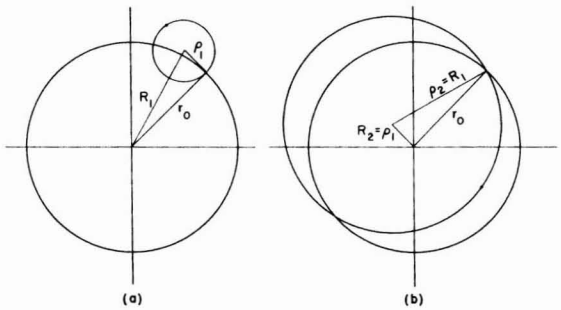

FIG. 3. Projections of helical electron orbits on a z = constant plane upstream (a) and downstream (b) of the cusp transition.

from the axis of a cylindrical coordinate system. This equation of motion can easily be found to be

$$\ddot{r} + \frac{r\omega^2}{4}\left(1 - \frac{(R^2 - \rho^2)^2}{r^4}\right) = 0. \tag{8}$$

By direct comparison of Eqs. (7) and (8):

$$R^2 - \rho^2 = r_0^2, \qquad (R > \rho), \tag{9a}$$

$$\rho^2 - R^2 = r_0^2, \qquad (R < \rho), \tag{9b}$$

$$\omega = \omega_c. \tag{9c}$$

Therefore, the motion of the electrons can be seen to be helical orbits of angular frequency ω_c with centers of gyration and Larmor radii related by Eqs. (9a) and (9b).

The conservation of canonical angular momentum (3) dictates that particle motion upstream of the cusp must be off-axis ($R > \rho$) rotation. Downstream of the cusp, the motion of the electrons encircles the axis of symmetry ($R < \rho$). Projections of the helical orbits onto a z = constant plane upstream and downstream of the cusp transition are shown in Fig. 3.

The total particle velocity v_0 in the static magnetic field is a constant of the motion and may be written

$$v_0^2 = v_{z1}^2 + \rho_1^2\omega_c^2 = v_{z2}^2 + \rho_2^2\omega_c^2. \tag{10}$$

Making use of (6), this reduces to

$$\rho_2^2 = r_0^2 + \rho_1^2 = R_1^2, \tag{11a}$$

$$R_2^2 = \rho_2^2 - r_0^2 = \rho_1^2. \tag{11b}$$

Thus, a solution for the radial motion of the electrons in terms of the upstream Larmor radius ρ_1 has been found. The off-centering of particle orbits in the downstream region is identically equal to the Larmor radius of the particle in the upstream region, as shown in fig. 4. The direction of off-centering is determined by the instantaneous electron position at the cusp transition, and may be quite random in any actual experiment. In this case the maximum width of a beam of electrons in the downstream region would be twice the maximum upstream Larmor radius. In the following sections, this particle off-centering due to a nonzero radial component of velocity in the upstream region will be referred to as "incoherent off-centering" of particle orbits.

B. Nonideal cusp

A more realistic model for an experimental cusp is the form of the hyperbolic tangent. As expected, however, solutions to Lagrange equations for such a nonideal cusp become

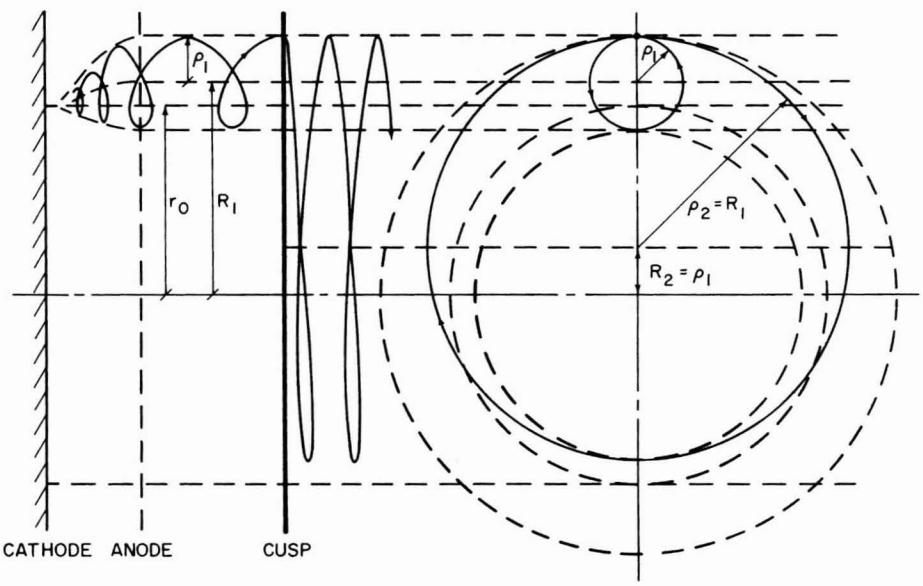

FIG. 4. Schematic of "incoherent off-centering" of particle orbits.

much more difficult to find. Nevertheless, first-order solutions may be found if restrictions on the initial conditions are applied.

If the magnetic field configuration takes the form

$$B = B_{z_0} f(z),$$

then

$$A_\theta = \frac{rB_{z_0}}{z} f(z),$$

where $f(z)$ is an arbitrary function with the property that

$$\lim_{z \to \pm\infty} f(z) = \mp 1.$$

Under the assumptions that $r \cong r_0$ (central ray) and $\dot{r}/r_0\omega_c \ll 1$ during the cusp transition, the first-order Lagrange equations corresponding to Eqs. (4), (5), and (7a) may be written

$$\dot{\theta} = \frac{\omega_c}{2}(f - 1), \tag{12a}$$

$$\ddot{z} + \left(\frac{\omega_c r_0}{2}\right)^2 (f - 1) f' = 0, \tag{12b}$$

$$\ddot{r} + r_0 \left(\frac{\omega_c}{2}\right)^2 (f^2 - 1) = 0 \tag{12c}$$

where the prime denotes d/dz. The equation for the axial motion in the transition region may be integrated to yield the axial velocity as a function of z

$$v_z(z) = \frac{r_0\omega_c}{2}[(2\eta)^2 - q^2]^{1/2} \tag{13}$$

where $\eta = v_0/r_0\omega_c$ and $q = 1 - f$. Using the relation

$$\frac{d}{dt} = v_z \frac{d}{dz}$$

and substituting (13) into (12c) yields an expression for the radial velocity gained in the cusp transition

$$\dot{r} = \int_0^2 \frac{\omega_c}{2} \frac{f^2 - 1}{[(2\eta)^2 - q^2]^{1/2} f'} dq. \tag{14}$$

The real experimental field is modeled using the relation

$$f = -\tanh \frac{z}{\zeta}$$

where ζ is a scale factor to fit the theoretical field to the actual experimental values. Then,

$$f' = -\frac{1}{\zeta}\left(1 - \tanh^2 \frac{z}{\zeta}\right) = \frac{f^2 - 1}{\zeta}. \tag{15}$$

Equation (14) can then be integrated to yield

$$\dot{r} = \frac{\zeta\omega_c}{2} \sin^{-1} \frac{1}{\eta}. \tag{16}$$

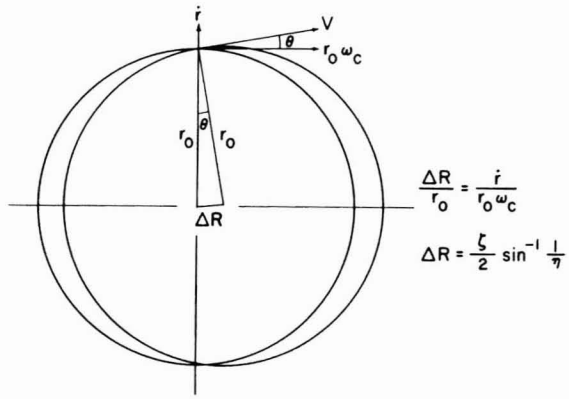

FIG. 5. Geometry of "coherent off-centering" of particle orbits.

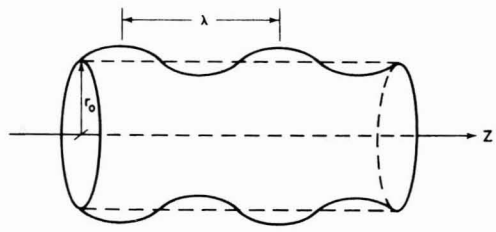

FIG. 6. Beam envelope downstream of the cusp transition for a hollow beam of electrons of small energy spread.

Figure 5 is useful in finding the new center of gyration

$$\Delta R = \frac{\dot{r}}{\omega_c} = \frac{\zeta}{2} \sin^{-1} \frac{1}{\eta}. \tag{17}$$

It can be seen that the direction of ΔR is nearly 90° from the point where the electron passes through the cusp since $\theta \ll 1$. The nature of this off-centering is quite different from the incoherent off-centering described in the last section. All of the particles passing through the cusp will be off-centered an amount ΔR in the direction 90° from the point where they pass through the cusp. As a result, this off-centering is referred to as "coherent off-centering" of particle orbits in subsequent sections of this paper. As a result of this off-centering, a hollow beam of electrons of small energy spread would be expected to have a beam envelope downstream of the cusp as shown in fig. 6. The wavelength λ of such an envelope would be given by

$$\lambda = \frac{2\pi v_{z2}}{\omega_c} = \frac{2\pi(v_{z1}^2 - r_0^2\omega_c^2)^{1/2}}{\omega_c} = 2\pi r_0(\eta^2 - 1)^{1/2}. \tag{18}$$

III. EXPERIMENT

A. Experimental apparatus

The experiments were performed in the cusped magnetic field in the University of Maryland Electron Ring Accelerator project. The general experimental configuration is shown in Fig. 7. In the experiment, two opposing solenoids are used to form a magnetic cusp. The transition width of the cusp is narrowed substantially by a soft iron plate placed between the solenoids. Measurements of the axial and radial magnetic field components through the cusp region indi-

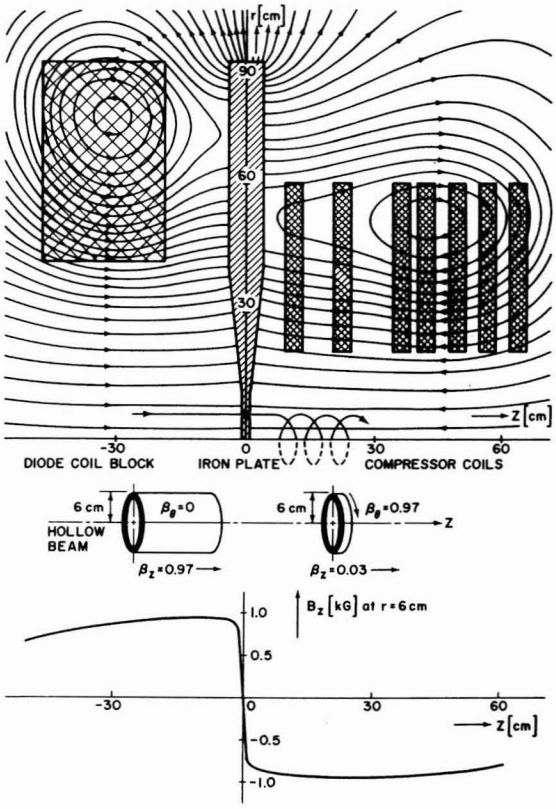

FIG. 7. General experimental configuration.

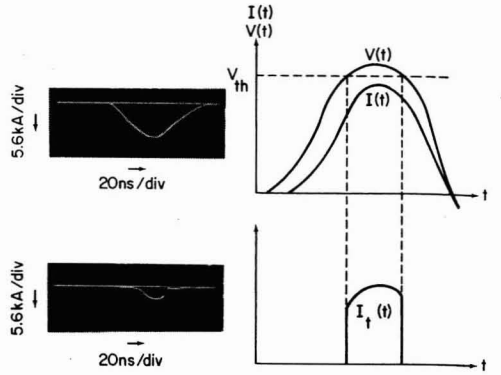

FIG. 8. Threshold energy measurements. Faraday cup current waveforms upstream and downstream of the cusp transition show the predicted narrowing of the current pulse in time downstream of the cusp.

cate that the cusp transition width is about 1.5 cm. A hollow, relativistic electron beam is emitted from a circular knife-edge cathode approximately 10 cm upstream of the iron plate. An aluminum plate attached to the surface of the iron plate serves as the anode. The cusp region is sufficiently narrow so that the electron motion in this region is essentially nonadiabatic and the electrons primarily see the $v_z \times B_r$ force in the transition region. This force acts to convert the axial beam velocity on the diode side of the cusp into rotational velocity on the downstream side, as shown in the figure. The electrons pass through a 0.5 cm wide annular slit in the iron plate. Typical diode voltage and current are 1–2 MV and 4–10 kA, respectively. The magnitude of the magnetic field on the diode side was set equal to that on the downstream side, and for these experiments was in the range 500–1500 G. The experimental current densities are sufficiently low so that the magnetic self-fields of the electron beam are only about 10% of the applied fields. The pulse width at half maximum of the electron beam on the diode side was about 35 nsec.

One distinguishing feature of these experiments is that they were performed at a sufficiently good vacuum (about 10^{-5} Torr) to insure that charge neutralization of the electron beam is negligible both upstream and downstream of the cusp. Previous work in this area[7–9] was performed under conditions where the electron beam was completely charge neutralized in the downstream region.

B. Threshold energy measurements

A low-inductance Faraday cup was used to investigate the total current transmitted through the cusp. The theoretical analysis described previously predicts the existence of a threshold energy below which electrons will be reflected at the cusp. The threshold velocity, equal to

$$v_{zth} = r_0\omega_c,$$

may be rewritten in terms of particle energy

$$E_{th}(\text{Joules}) = [(m_0c^2)^2 + c^2e^2r_0^2B^2]^{1/2} - m_0c^2$$

or in laboratory units

$$E_{th}(\text{MeV}) = [0.261 + 8.989 \times 10^{-2}r_0^2B^2]^{1/2} - 0.511$$

with units of r_0 and B in centimeters and kiloGauss, respectively. This reflection of lower energy electrons should result in a narrowing of the current pulse in time downstream of the cusp, as shown schematically in Fig. 8. Oscilloscope traces of the Faraday cup current collected on both sides of the cusp are shown in the same figure for comparison, and clearly show the narrowing of the current pulse in time predicted by the theory. In this case, the magnetic field was set to a value somewhat below the theoretically predicted cutoff value for the peak energy electrons. By raising the magnetic field on both sides of the cusp to beyond this cutoff value, electron transmission through the cusp can be almost entirely cut off. In this manner, it is possible to generate very short duration (less than 10 nsec) pulses of relativistic electrons with correspondingly low energy spread. The loss in peak current amplitude through the cusp is a result of collective effects on the diode side, and will not be discussed in this paper.

C. Incoherent off-centering of particle orbits

The incoherent off-centering of particle orbits arising from a nonzero radial component of particle velocity at the diode has been investigated using both time-integrated and time-resolved techniques. Time-integrated photographs of the beam cross section 5 cm and 20 cm downstream from the iron plate have been obtained by photographing the light emitted when the beam strikes a graphite covered glass plate. Two separate shots were required to obtain these photographs and the results are shown in Fig. 9. While time-integrated, these photographs clearly show the beam cross section to have spread considerably in the 15 cm of travel between the observation points. A useful measure

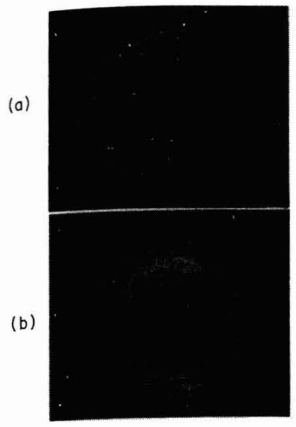

FIG. 9. Time-integrated photographs of the beam cross section 5 cm (a) and 20 cm (b) downstream of the cusp transition.

of the effect of the self-fields of an electron beam on the orbits of the beam electron is the ratio ν/γ, which is equal to the ratio of the beam current to the Alfvén[13] current limit ($17\,000\beta\gamma$). The low ν/γ of the downstream electron beam in these experiments is a strong indication that the beam spreading is not due to collective effects. Time-resolved study of the beam cross section, moreover, indicates that incoherent off-centering of particle orbits may be important in explaining the beam spreading.

The analysis in Sec. II of this paper can be used to construct a theoretical picture of the beam cross section as a function of time a distance z_0 downstream of the cusp transition. Equations (6) and (10) yield an expression for the axial velocity downstream of the cusp in terms of the total velocity v_0 after acceleration in the diode and ρ_1, the upstream Larmor radius

$$v_{z2} = (v_0^2 - \omega_c^2 r_0^2 - \omega_c^2 \rho_1^2)^{1/2}.$$

The time-of-flight from the cusp transition to the downstream observation point a distance z_0 from the cusp transition is given by

$$t_f = \frac{z_0}{v_{z2}} = z_0[r_0\omega_c(\eta^2 - 1 - \rho^2_{1/r_0^2})^{1/2}]^{-1}.$$

If the departure time of an electron from the cusp transition is denoted by t_d, where t_d is determined empirically from the diode voltage waveform, then the electron will arrive at the point downstream of the cusp at a time given by

$$t = t_d + t_f.$$

Plots of this arrival time as a function of ρ_1 (normalized to r_0) for $B = 800$ G, $z_0 = 20$ cm and several different electron energies have been constructed and are shown in Fig. 10. As no restrictions have been placed on the possible magnitude of ρ_1 other than the requirement that $\rho_1\omega_c$ not exceed v_0, the actual experimental data can be expected to lie somewhere inside the general profile shown if the peak electron energy does not exceed 1.6 MeV.

Figure 11 shows the experimental configuration used for the time-resolved studies of the beam cross section. The electron beam travels a distance z_0 downstream of the iron plate and strikes a thin scintillating rod. The scintillation

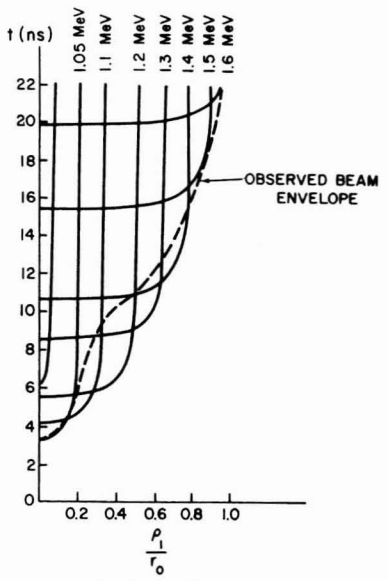

FIG. 10. Predicted arrival time of electrons at the observation point ($z_0 = 20$ cm) downstream of the cusp transition plotted as a function of the upstream Larmor radius ρ_1 for several different electron energies. The observed beam envelope is also shown to the same scale.

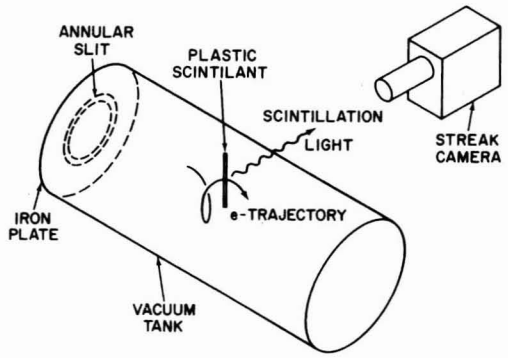

FIG. 11. Experimental configuration used for the time-resolved studies of the beam cross section.

light from the rod is photographed with the use of an image converter camera operating in the streak mode. A typical streak picture is shown in Fig. 12. It can be seen that early in time the beam cross section is well defined, and that the spreading occurs later in the pulse. The envelope of the streak photograph has been scaled to the theoretically predicted envelope and plotted in Fig. 10. Given the assumptions made in the first-order theoretical analysis, the experimental results are in reasonable agreement with the theoretical expectations.

D. Coherent off-centering of particle orbits

Figure 13 shows the experimental configuration used to study the coherent off-centering of particle orbits. A mask was used to block most of the electron beam before the cusp transition. A small pinhole in the mask allowed a small section of the beam (typically 1 mm^2) to pass through the cusp transition region. A film plate was placed downstream of the cusp in the $r - z$ plane, and was moved azimuthally

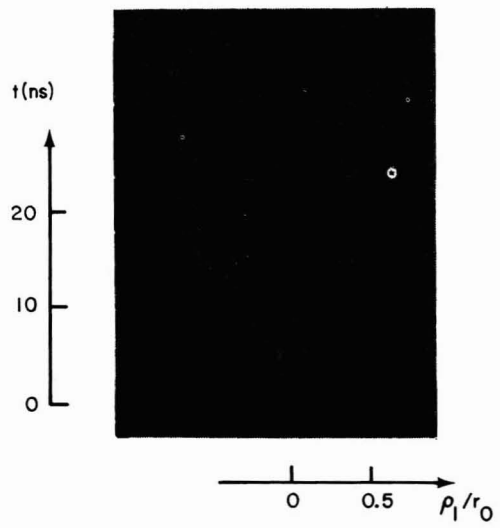

FIG. 12. Typical streak photograph of the beam cross section.

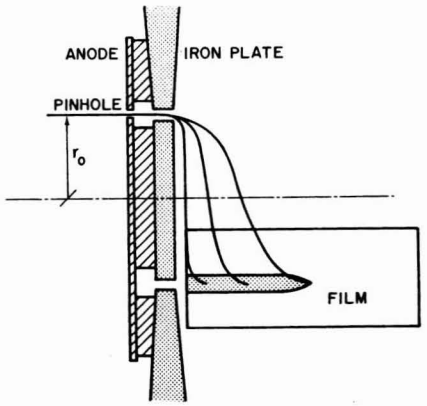

FIG. 13. Experimental configuration used for the study of "coherent off-centering" of particle orbits.

from shot to shot. At the point where they struck the film, the helical orbits of the most energetic electrons would extend farther downstream than the lower energy particles, and the resulting track on the film was used to analyze the particle behavior. An actual film from the experiment is also shown.

Figure 14 shows a plot obtained from the "single-particle" experiments. Here, the axial distance traveled by the peak energy particle is plotted as a function of azimuthal angle. For the low field case (B = 832 G), the magnetic field was well below the theoretically predicted cutoff value for 1.5 MeV electrons, and the orbits of the electrons in the downstream field were simple helices. For the high field case (B = 1000 G), the field was close to the predicted value, and the particles were slowed and finally reflected in the rising magnetic field of the downstream side of the cusp. From this result, the ratio of total velocity to azimuthal velocity can be found and compared to the theoretical result given in Eq. (6).

In Sec. II it was shown that the finite width of the cusp transition gives rise to a coherent off-centering of particle

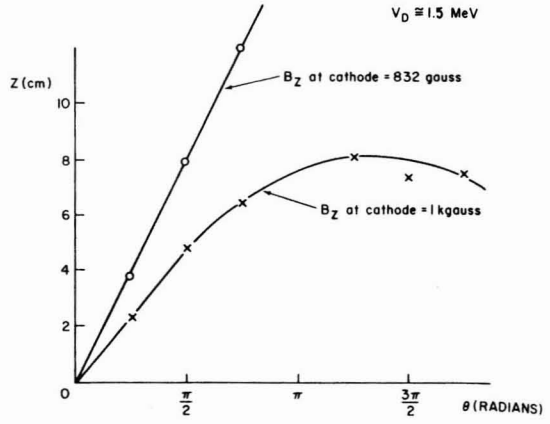

FIG. 14. Plot of axial distance traveled downstream of the cusp for the peak energy electron as a function of azimuthal angle. Data is shown for two different magnetic field strengths.

orbits in a direction 90° from the point at which the electrons pass through the cusp. The amount of this off-centering was found to be

$$\Delta R = \frac{\zeta}{2} \sin^{-1} \frac{1}{\eta} .$$

The scale factor ζ was carefully determined by fitting the experimental field to the theoretical model ($\zeta = 0.907$ in the experiment), and actual experimental operating conditions were used to calculate the predicted off-centering.

Figures 15 and 16 show projections of the helical electron orbits into a z = constant plane, as obtained from the experimental data. The orbits can be seen to be nearly circular with radius 6 cm, which is equal to the mean radius of the annular slit in the iron plate through which the beam passes. The off-centering of these orbits in the direction 90° from the pinhole is about 2 mm in the low field case and 6 mm in the high field case.

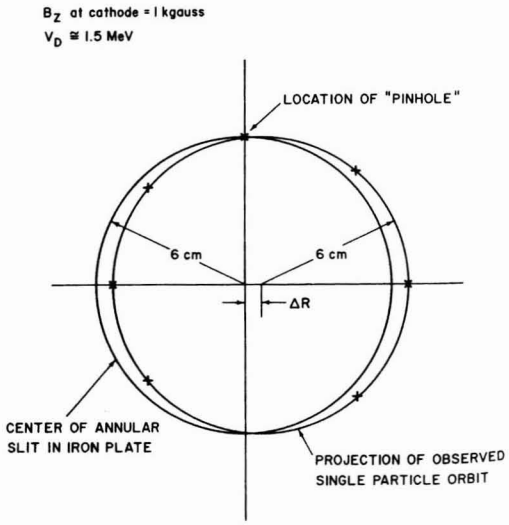

FIG. 15. Projection of helical electron orbit downstream of the cusp onto a z = constant plane, as obtained from the experimental data. B = 1000 G.

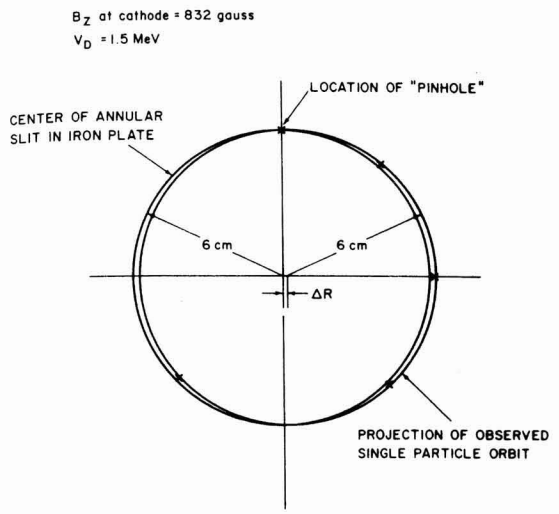

FIG. 16. Projection of helical electron orbit downstream of the cusp onto a z = constant plane, as obtained from the experimental data. B = 832 G.

TABLE I. Comparison of theoretical and experimental results for typical experimental parameters.

B_z	η_{theor}	η_{meas}	ΔR_{theor}	ΔR_{meas}
832 G	1.30	1.31	0.39 cm	0.2 cm
1000 G	1.08	1.13	0.53 cm	0.6 cm

Table I summarizes the results of these experiments. The ratio of total to azimuthal velocity η calculated from single-particle theory is in good agreement with the experimental result. The predicted off-centering ΔR is also in reasonable agreement with the experimental results, with differences likely due to experimental error and the assumptions made in the first-order analysis.

IV. CONCLUSIONS

An experiment to investigate the trajectories of relativistic electrons in the presence of a cusped magnetic field has been performed and the results compared with theoretical expectations. The current densities in the experiment reported here are sufficiently low so that the self-magnetic fields of the electron beam are only about 10% of the applied fields. Thus, single-particle theory is sufficient to explain the overall beam behavior in the cusp transition. The Lagrangian formulation has been used to solve for the electron trajectories in some simple magnetic cusp configurations. A threshold energy for transmission through the cusp has been observed and is in reasonable agreement with the predicted result. Two different electron orbit off-centering mechanisms, referred to here as incoherent and coherent, have been observed experimentally and found to conform to theoretical expectations.

ACKNOWLEDGMENTS

The authors are grateful to Professors H. Kim, M. P. Reiser, and G. T. Zorn for many helpful discussions. D. W. Hudgings rendered valuable assistance in the design and construction of the experiments, as well as help in the data acquisition. C. N. Boyer and P. K. Misra also assisted in the experimental work. H. S. Uhm assisted in the analytical calculation of the "coherent off-centering" of particle orbits. Valuable technical assistance was rendered by C. A. Meese and R. J. Hendron.

This work was supported by the National Science Foundation under Contract GP-29706.

[1] G. Schmidt, Phys. Fluids **5,** 994 (1962).
[2] J. Sinnis and G. Schmidt, Phys. Fluids **6,** 841 (1963).
[3] D. L. Nelson, Ph.D. dissertation, University of Maryland (1970); see, also D. L. Nelson and H. Kim, in *Proceedings of VII International Conference on High Energy Accelerators* (Publishing House of the Academy of Sciences of Armenian SSR, Yerevan, 1970), p. 540.
[4] J. G. Kalnins, H. Kim, and D. L. Nelson, IEEE Trans. NS-**18,** 473 (1971).
[5] M. P. Reiser, IEEE Trans. NS-**18,** 460 (1971).
[6] M. P. Reiser, IEEE Trans. NS-**20,** 310 (1973).
[7] M. Friedman, Phys. Rev. Lett. **24,** 1098 (1970).
[8] C. A. Kapetanakos and W. M. Black, Bull. Am. Phys. Soc. **18,** 1264 (1973).
[9] R. E. Kribel, K. Shinsky, D. A. Phelps, and H. H. Fleischmann, Bull. Am. Phys. Soc. **17,** 999 (1972).
[10] M. J. Rhee and G. T. Zorn, in *Proceedings of VIII International Conference on High Energy Accelerators* (CERN-Scientific Information Service, Geneva, 1971), p. 481.
[11] W. W. Destler, D. W. Hudgings, J. G. Linhart, P. K. Misra, M. P. Reiser, M. J. Rhe, and G. T. Zorn, Bull. Am. Phys. Soc. **18,** 1265 (1973).
[12] M. J. Rhee, W. W. Destler, D. W. Hudgings, M. P. Reiser, H. S. Uhm, and G. T. Zorn, Bull. Am. Phys. Soc. **18,** 1265 (1973).
[13] H. Alfvén, Phys. Rev. **55,** 425 (1939).